American Mineralogist, Volume 80, pages 968–981, 1995

Experimental evidence for the exsolution of ilmenite from titaniferous spinel

Dominique Lattard
Fachgebiet Petrologie, Technische Universität Berlin, EB 310, Strasse des 17. Juni 135, D-10623 Berlin, Germany

Abstract

Microintergrowths of titaniferous spinel and ilmenite have been experimentally produced in the system Fe-Ti-Cr-O by annealing in vacuo at constant temperatures in the range 700–1100 °C of spinel + ilmenite assemblages previously synthesized at 1300 °C under controlled low f_{O_2}. Depending on the original f_{O_2} of synthesis at 1300 °C, annealing produces three types of microintergrowths: Type I (lowest f_{O_2}: 10^{-11}) has rims and trellis-like lamellae of ilmenite as well as small blebs of metallic iron; type II (f_{O_2}: 10^{-10}–10^{-9}) shows spinel with rims and a few lamellae of ilmenite; type III (highest f_{O_2}: $10^{-8.5}$) displays both spinel with rims and lamellae of ilmenite and ilmenite with rims and lamellae of spinel.

On the basis of microprobe analysis, including precise determination of the O contents, it is shown that the synthetic microintergrowths did not form by a redox process. Rather, the textures represent exsolution caused by vacancy relaxation in spinel (and, for the most reduced samples, in ilmenite), according to the substitution scheme

$$Fe_2^{2+}Ti_{-1}^{4+}\square_{-1}. \quad (1)$$

The presence of metallic iron in the most reduced samples (type I) results from the shift of the iron saturation surface toward more Fe-rich compositions with decreasing temperature. The rims and lamellae of spinel around and within ilmenite in the type-III samples result from the combination of Exchange 1 and the well-known substitution $Fe^{2+} + Ti^{4+} = 2Fe^{3+}$.

These experimental results show that natural spinel + ilmenite microintergrowths do not always result from either an oxidation or a reduction process. In particular, textures similar to those of type I, which were observed in lunar basalts, may simply record cooling under O_2-conserving conditions. In most terrestrial rocks, however, spinel + ilmenite intergrowths are certainly best interpreted as resulting from oxidation of at least a subsystem of the rock.

Introduction

Intergrowths of titaniferous spinel (ulvöspinel, titanomagnetite, or magnetite) with ilmenite are widespread in igneous and metamorphic rocks, both of terrestrial and lunar origin (e.g., reviews in Frondel, 1975; Lindsley, 1991; Haggerty, 1991a, 1991b). Buddington and Lindsley (1964) recognized several textural types of such intergrowths in terrestrial rocks: (1) "trellis intergrowths of thin ilmenite lamellae in all sets of (111) planes of the host" spinel; (2) "sandwich intergrowths of thick ilmenite lamellae predominantly in one set of (111) planes"; (3) ilmenite granules within the spinel; and (4) "granules or occasional lamellae of ilmenite on the external borders" of the spinel "or recrystallized granular aggregates of ilmenite" and spinel.

On the basis of experimental work in the Fe-Ti-O system (Lindsley, 1962, 1963), Buddington and Lindsley (1964) clearly demonstrated that all these intergrowths can be formed by oxidation of the Fe_2TiO_4 (ulvöspinel) component in titanomagnetite during cooling, although types 3 and 4 can also be caused by contemporaneous crystallization of ilmenite and spinel. This explanation contradicted the long-accepted hypothesis that $FeTiO_3$ enters into solid solution with magnetite at high temperature and exsolves upon cooling (e.g., Ramdohr, 1955, p. 153).

The microintergrowths of Al- and Cr-bearing ulvöspinel or Al- and Ti-bearing chromite with ilmenite in lunar basalts resemble those of terrestrial rocks, except that they often contain blebs or lamellae of iron. These textures were attributed by several authors to late-stage subsolidus reduction (e.g., El Goresy et al., 1972; Haggerty, 1972, 1977). Haselton and Nash (1975), however, proposed an alternative, O_2-conserving model involving the exsolution of the Ti^{3+}-component in ilmenite accompanied by the formation of iron.

The present experimental study was originally designed to model the effect of posteruptive cooling in lunar mare basalts on the composition of coexisting iron titanium oxides (Lattard and Woermann, 1987). For this purpose, spinel + ilmenite assemblages synthesized in the Fe-Ti-

0003–004X/94/0910–0968$02.00

Cr-O system at 1300 °C under reducing conditions were subsequently annealed at lower temperatures in evacuated silica-glass tubes, i.e., supposedly under O_2-conserving conditions. In most annealed samples, ilmenite was found to form lamellae within spinel grains and rims around these grains, in some cases in association with iron. The interpretation was thus conflicting: If O_2-conserving conditions were maintained during the experiments, only an exsolution process could be envisaged, which appeared to contradict the well-founded arguments of Buddington and Lindsley (1964). On the other hand, if the silica-glass tubes did allow O_2 exchange with the surrounding atmosphere, oxidation should have occurred, but this did not fit with the appearance of iron in some of the spinel-ilmenite intergrowths.

This dilemma was resolved by analyzing the coexisting spinels and ilmenites for O, as well as the cations, using an electron microprobe. The analyses show that spinel + ilmenite microintergrowths can indeed be formed by exsolution processes accompanying vacancy relaxation in spinel upon cooling from high temperatures. The present paper presents details of the experimental methods, analytical results, and the deduced mechanisms of intergrowth formation. A subsequent publication will deal with the textural and chemical evolution of these spinel + ilmenite assemblages as a function of time and annealing temperature.

Four models to explain the formation of ilmenite + spinel microintergrowths

Before explaining the experimental work, it is useful to compare in a graphical representation the four models proposed in the literature for the formation of ilmenite + spinel microintergrowths. Although the FeO-Fe_2O_3-TiO_2 and the FeO-$FeO_{1.5}$-TiO_2 triangles have been widely used in the petrological literature (e.g., Lindsley, 1991), the Fe-Ti-O diagram (e.g., Grey et al., 1974; Merritt and Turnbull, 1974) is more appropriate to compare redox vs. O_2-conserving processes.

In the Fe-Ti-O system, spinel, ilmenite, and pseudobrookite display extensive solid solutions (Fig. 1a). Along all three joins the main substitution scheme is $2Fe^{3+} = Fe^{2+} + Ti^{4+}$ (see review in Lindsley, 1991). At high temperatures the solid solutions may expand beyond the end-members ulvöspinel, ilmenite, and "ferropseudobrookite" toward the corresponding Ti^{3+}-bearing end-members by means of the substitution $Ti^{3+}_2Fe^{2+}_{-1}Ti^{4+}_{-1}$. The degree of Ti^{3+} substitution in ulvöspinel$_{ss}$ and ilmenite$_{ss}$ appears to be small, although opinions vary regarding the exact extent of the substitution (Grey et al., 1974; Simons and Woermann, 1978; Borowiec and Rosenqvist, 1985).

Figure 1b shows a portion of the spinel and ilmenite joins with a schematic representation of the widths of both phases in the direction of cation deficiency. There is serious disagreement among investigators concerning the amount of cation deficiency (e.g., MacChesney and Muan, 1961; Webster and Bright, 1961; Taylor, 1964; Grey et al., 1974; Simons and Woermann, 1978; Dieckmann, 1982; Senderov et al., 1993). Detailed studies on magnetite have shown that the vacancy concentration is positively correlated with temperature, and that it is negligible below 900 °C (e.g., Dieckmann, 1982). No cation excess has been reported for either Fe_2TiO_4-rich spinel or $FeTiO_3$-rich ilmenite.

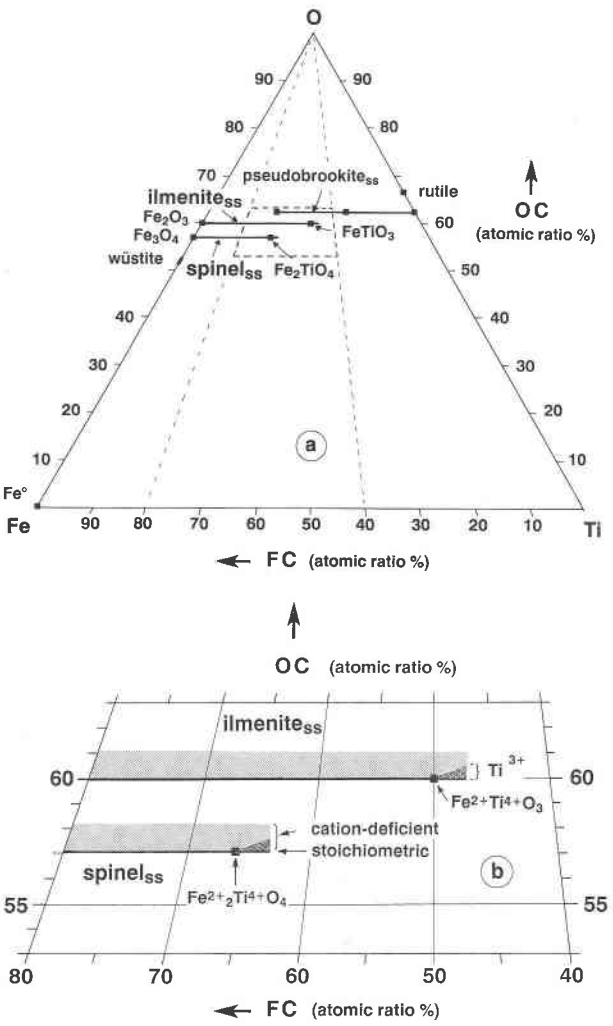

Fig. 1. Schematic representation of selected phases in the system Fe-Ti-O. (**a**) Complete Fe-Ti-O diagram showing only phases with stoichiometric compositions (except for wüstite), with some end-member compositions (black squares). Thick horizontal lines show the maximum extent of solid solution at high temperature for pseudobrookite$_{ss}$, ilmenite$_{ss}$, and spinel$_{ss}$, according to the substitution schemes $2Fe^{3+} = Fe^{2+} + Ti^{4+}$ and $2Ti^{3+} = Fe^{2+} + Ti^{4+}$. In the case of pseudobrookite$_{ss}$, the solid solution toward end-member anosovite (Ti_3O_5) is complete only at temperatures above ca. 1350 °C (Ender et al., 1980; Grey and Merritt, 1981). (**b**) Enlarged portion of the dashed trapezoid shown in **a**. The pseudobrookite solid solution is omitted for clarity. Black lines represent stoichiometric compositions, light-stippled areas indicate cation-deficient compositions (schematic), and heavy-stippled triangles denote cation-deficient compositions containing Ti^{3+}. FC = 100Fe/(Fe + Ti), OC = 100O/(O + Fe + Ti).

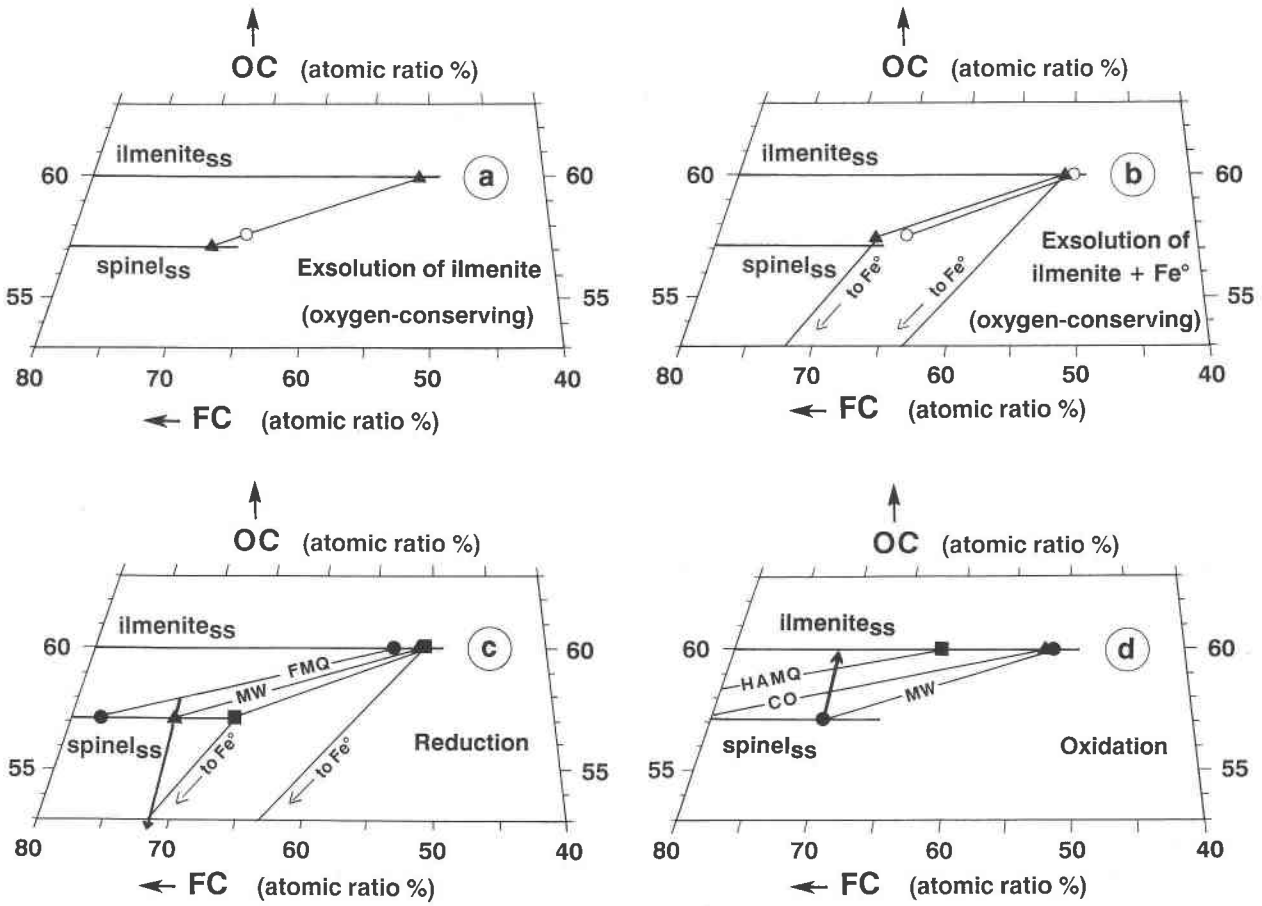

Fig. 2. Schematic representation of four models for the explanation of the formation of ilmenite exsolution in spinel, using the same type of diagram as Fig. 1b. (**a**) Exsolution of the $FeTiO_3$ component in spinel (after Ramdohr, 1955). Open circle: composition of defect spinel (i.e., spinel containing some $FeTiO_3$-component); solid triangles: compositions of stoichiometric spinel$_{ss}$ and ilmenite$_{ss}$ deriving from the defect spinel. (**b**) Exsolution of the Ti^{3+} component in ilmenite (after Haselton and Nash, 1975). Open circles: spinel$_{ss}$ and ilmenite$_{ss}$ coexisting at high temperature; solid triangles: spinel$_{ss}$ and ilmenite$_{ss}$ in equilibrium with iron at lower temperature. (**c**) Reduction (after El Goresy et al., 1972; Haggerty, 1972, 1977). Squares: spinel$_{ss}$ and ilmenite$_{ss}$ in coexistence with metallic iron (Simons and Woermann, 1978); triangles: spinel$_{ss}$ and ilmenite$_{ss}$ stable on the MW buffer; solid circles: spinel$_{ss}$ and ilmenite$_{ss}$ stable on the fayalite + quartz + magnetite buffer (FMQ). The arrow indicates the reduction path from a spinel + ilmenite assemblage (FMQ), through single spinel (MW), toward the spinel + iron and the spinel + ilmenite + iron assemblages. All data are from experiments at 1000 °C (pressures in the range 1 bar–2 kbar). Those for the MW and FMQ buffered experiments are from Lindsley (1962, 1963), as given in Ghiorso (1990). (**d**) Oxidation (after Buddington and Lindsley, 1964). Solid circles: compositions of spinel$_{ss}$ and ilmenite$_{ss}$ coexisting under the f_{O_2} of the magnetite + wüstite buffer (MW); triangle: ilmenite$_{ss}$ in equilibrium with a spinel$_{ss}$ under the f_{O_2} of the Co + CoO buffer (CO); square: ilmenite$_{ss}$ in equilibrium with a spinel$_{ss}$ under the f_{O_2} of the hedenbergite + andradite + magnetite + quartz buffer (HAMQ). In the case of the last two buffers, the spinels plot outside of the diagram. The arrow indicates the oxidation path of a spinel$_{ss}$ synthesized on the MW buffer. All spinel$_{ss}$ and ilmenite$_{ss}$ compositions are from experiments at 800 °C and pressures of 1 or 2 kbar. Data are from Lindsley (1962, 1963), Andersen and Lindsley (1988), and Spencer and Lindsley (1981), as listed in Ghiorso (1990).

Of the four model processes proposed for the formation of ilmenite-spinel intergrowths, two (a and b) are O_2 conserving and two (c and d) involve redox processes (Fig. 2): (a) Exsolution of the $FeTiO_3$ component in spinel (e.g., Ramdohr, 1955) occurs when a cation-deficient (high-temperature) spinel becomes stoichiometric at lower temperature by exsolving stoichiometric ilmenite (Fig. 2a). (b) Exsolution of ilmenite and metallic iron from ilmenite-ulvöspinel parageneses (Fig. 2b) is related to the shift of the ulvöspinel$_{ss}$-ilmenite$_{ss}$-iron three-phase-field toward Fe-rich compositions with decreasing temperature (Simons and Woermann, 1978). The model proposed by Haselton and Nash (1975) involves Ti^{3+}-bearing ilmenite and is modeled by the reaction

$$\underset{\text{ilmenite}_{ss}}{[9FeTiO_3 + Ti_2O_3]} + \underset{\text{ulvöspinel}}{3Fe_2TiO_4} = \underset{\text{ilmenite}}{14FeTiO_3} + \underset{\text{iron}}{Fe^0}.$$

(c) Reduction of a spinel rich in the ulvöspinel compo-

nent leads to a Ti-richer spinel accompanied by a small amount of ilmenite and iron (Fig. 2c). In principle, this is the mechanism used to explain microintergrowths of chromian (aluminian) ulvöspinel with ilmenite and iron in lunar basalts (e.g., El Goresy et al., 1972; Haggerty, 1972, 1977). (d) Oxidation of any spinel on the join magnetite-ulvöspinel produces a magnetite-enriched spinel and a coexisting ilmenite$_{ss}$ (Fig. 2d). This is the "Oxy-exsolution" of Buddington and Lindsley (1964). With decreasing temperature, the amount of ilmenite produced increases because the tie lines become flatter (Fig. 2d).

Experimental methods

Preparation of the samples

The samples were prepared in two steps: (1) Polycrystalline ulvöspinel$_{ss}$ + ilmenite$_{ss}$ assemblages were synthesized from oxide mixtures in the system Fe-Ti-Cr-O at 1300 °C under various low oxygen fugacities (starting samples); (2) fragments of these starting samples were annealed at lower temperatures in vacuo for different experiment durations (annealed samples).

Bulk composition of the samples. Because the mare basalt spinels are dominantly solid solutions between the ulvöspinel and the chromite end-members (El Goresy, 1976), the experiments were performed in the Fe-Ti-Cr-O system. Of the different bulk compositions originally prepared, the composition designated "Ki-1" was used for all experiments reported here because it leads (at 1300 °C) to assemblages comprising only ilmenite$_{ss}$ and ulvöspinel$_{ss}$ in roughly equal quantities (see phase relations in Knecht et al., 1977).

The starting mixtures were prepared from the following reagents: Fe_2O_3 (Merck no. 3924; p.a., minimum 99%), TiO_2 (Merck no. 808; minimum 99%), and Cr_2O_3 (Riedel de Haen no. 12233; "rein," minimum 99.8%). A 10 g mixture of these reagents was weighed, thoroughly ground and mixed under acetone, and dried overnight at 120 °C. Batches of 1–2 g of these mixtures were pressed into pellets, which were annealed in air for 1 d at 1050 °C.

Synthesis of Cr-rich ulvöspinel$_{ss}$ + ilmenite$_{ss}$ assemblages at 1300 °C under controlled f_{O_2} (starting samples). To synthesize the Cr-rich ulvöspinel$_{ss}$ + ilmenite$_{ss}$ starting assemblages, the pellets were fired for 1 d at 1300 °C in vertical furnaces (Pyrox). Oxygen fugacities in the range 10^{-11}–$10^{-8.5}$ were fixed by mixing high-purity H_2 and CO_2 gas. The mixing ratios were taken from Deines et al. (1974), and the equipment was that devised by Darken and Gurry (1945) and described by Nafziger et al. (1971). At the end of the experiments, the samples were dropped from the hot zone of the furnace to the cool end, where they were quenched to room temperature in the H_2-CO_2 gas mixture. Previous work (Knecht et al., 1977) has shown that this cooling process is fast enough to conserve the high-temperature equilibrium state.

Annealing at lower temperatures under O_2-conserving conditions. To ensure O_2-conserving conditions for the annealing process, fragments of the starting samples were sealed in evacuated (vacuum $\leq 10^{-2}$ mbar) silica glass capsules. The inner volume of the capsules was minimized by using filling rods of silica glass. The capsules were heated in conventional vertical (Kanthal-wound) tube furnaces at constant temperatures in the range 700–1100 °C, with experiment durations between 0.5 h and 90 d. Care was taken not to surpass the critical experiment duration at which silica glass begins to recrystallize and becomes brittle (cf. empirical determination by Ender, 1976). The samples were quenched by rapid immersion of the silica glass capsules into cold water. Cooling was fast enough to preserve the high-temperature state (Knecht et al., 1977). Only dry samples were accepted for further investigation, thereby ensuring that the silica glass capsules remained gas tight and evacuated during the whole experiment and the quenching procedure.

In all furnaces the hot zone with a temperature range of ±1 °C was about 40 mm long. The temperature was controlled by commercial thyristor controllers to ±1 °C and measured before and after each experiment using Pt-$Pt_{90}Rh_{10}$ thermocouples calibrated against the melting points of gold and diopside. The temperature accuracy was estimated to be ±5 °C.

The phases in both the starting samples and the annealed samples were identified by X-ray diffractometry and microscopic investigation under reflected light in oil immersion. Because of the small grain size, backscattered electron images of polished samples were necessary to reveal textural details.

Analytical methods

Starting samples and annealed samples were analyzed by electron microprobe. For most analyses presented in the present paper, quantitative measurements of O, Fe, Ti, and Cr were performed. These analyses were made using a CAMECA SX50 electron microprobe equipped with standard WDS crystals plus an OVONYX OV-060A W/Si multilayer synthetic reflector (Ovonic Synthetic Materials).

The peak-background intensities of the $K\alpha$ lines for O, Fe, Ti, and Cr were measured with an accelerating voltage of 15 kV and a beam current of 20 nA. To improve the counting statistics, long acquisition times were chosen: 60 s for peak and 30 s for background intensities. The standards used were synthetic $MnTiO_3$ (O, Ti), natural fayalite (Fe), and natural eskolaite (Cr). Because O X-rays are strongly absorbed by the carbon coating on the sample surface, coating on specimens and standards was performed simultaneously to obtain the same thickness of the carbon film. A second source of absorbing carbon on the sample surface is a deposit of hydrocarbon, which polymerized under the electron beam. Because the thickness of the contaminant layer increases linearly with time, care was taken not to repeat any measurement on the same spot (especially on standards).

Structural formulae and valence states were calculated from the elemental concentrations (including O!) on a fixed O basis (four O atoms p.f.u. in ulvöspinel$_{ss}$, three in

TABLE 1. Microprobe analyses of ilmenite from starting samples synthesized at 1300 °C under different f_{O_2} (means and standard deviations)

Starting sample	Ki-1/1	Ki-1/2	Ki-1/3	Ki-1/4	Ki-1/5
log f_{O_2}	−11.0	−10.0	−9.5	−9.0	−8.5
No. of analyses	$n = 11$	$n = 13$	$n = 10$	$n = 13$	$n = 11$
Ti (wt%)	31.99(12)	30.94(5)	30.40(8)	29.86(6)	28.66(9)
Cr	2.39(7)	2.41(5)	2.47(6)	2.62(4)	3.15(7)
Fe	33.54(17)	34.96(9)	35.46(11)	35.77(13)	36.49(16)
O	31.80(10)	31.58(9)	31.48(8)	31.32(14)	31.19(10)
Total	99.72(15)	99.89(15)	99.81(13)	99.57(23)	99.49(20)
		Calculated on the basis of 3 atoms p.f.u.			
TiO_2 (wt%)	50.57(108)	49.46(93)	49.41(72)	48.80(11)	47.80(14)
Ti_2O_3	2.50(99)	1.94(85)	1.17(63)	0.90(99)*	—
Cr_2O_3	3.50(19)	3.52(6)	3.61(9)	3.83(7)	4.60(11)
Fe_2O_3	—	—	—	0.15(27)*	1.38(103)
FeO	43.15(21)	44.98(11)	45.61(14)	45.89(27)	45.70(90)
Ti^{4+} (cat)	0.955(18)	0.941(15)	0.943(12)	0.936(18)	0.921(3)
Ti^{3+}	0.053(21)	0.041(18)	0.025(13)	0.019(21)*	—
Cr^{2+}	0.069(2)	0.070(1)	0.072(2)	0.077(1)	0.093(2)
Fe^{3+}	—	—	—	0.003(5)*	0.027(20)
Fe^{2+}	0.906(7)	0.951(4)	0.968(4)	0.979(8)	0.979(24)
Total	1.984(7)	2.003(6)	2.008(5)	2.014(8)	2.020(7)
Ti_{tot} (cat%)	50.81(17)	49.00(5)	48.19(14)	47.43(12)	45.59(13)
Cr	3.50(9)	3.51(7)	3.60(9)	3.83(7)	4.62(11)
Fe_{tot}	45.69(21)	47.49(9)	48.21(13)	48.74(9)	49.79(12)
OC (at%)	60.19(9)	59.96(7)	59.90(5)	59.83(10)	59.77(8)
FC (at%)	47.44(19)	49.25(7)	50.01(13)	50.65(10)	52.10(15)

Note: numbers in parentheses = standard deviations (1σ). Abbreviations: cat = cation per formula unit, cat% = cation percent, at% = atom percent, OC = 100O/(O + Fe + Ti + Cr), FC = 100(Fe + ½Cr)/(Fe + Ti + Cr).

* Ti^{3+} and Fe^{3+} are never calculated together in a single analysis but appear in means of analyses with either Ti^{3+} or Fe^{3+}.

ilmenite$_{ss}$), assuming that Fe^{3+} and Ti^{3+} are mutually exclusive.

O was measured to at least the same degree of precision as the other elements. In homogeneous samples, the relative standard deviations of the elemental concentrations are typically better than 0.5% (see Tables 1 and 2). The lowest precision was attained in measuring the low Cr concentrations in ilmenite$_{ss}$ (with elemental Cr < 3 wt%, relative standard deviation up to 3%).

Using the PAP correction procedure (Pouchou and Pichoir, 1984) with standard absorption coefficients, the analytical accuracy of the electron microprobe analyses of O is highly dependent on the standard used. In the present case, O was calibrated on $MnTiO_3$, so that the O measurements on ilmenite$_{ss}$ seem satisfactory, judging from the sums of elemental concentrations between 99.5 and 99.9 wt% (Table 1). In contrast, the O values measured in ulvöspinel$_{ss}$ are apparently too low by about 1 wt% (cf. sums of elemental concentrations in Table 2). This results in structural formulae with cation excesses and, in many cases, relatively high Ti^{3+} contents, which are both improbable (see Fig. 1b). More generally, the determination of small Ti^{3+}, Fe^{3+}, or vacancy contents is extremely sensitive to the accuracy of the measured elemental concentrations. However, because the accuracy of our O measurements seems essentially biased by the Ti or Fe absorption coefficients (or both), and because the precision and reproducibility of these measurements are excellent, differences in the O contents of phases with very similar compositions can be accurately determined. This was applied to evidence differences in this content between samples synthesized at 1300 °C under different f_{O_2} or changes in the O content in spinel or ilmenite during annealing. On the basis of such measured changes in the O content, reliable estimates of the original vacancy concentration can be performed.

To avoid any possible instrumental drift, the phases to be compared were analyzed within a few hours, and the reproducibility was checked several times during the session. As will be shown, for most spinel samples the changes in the OC-ratio [OC = 100O/(O + Fe + Ti + Cr) in atom percent] during annealing are in the range 0.5–0.8% (Table 3), whereas the corresponding relative standard deviations for each sample are all <0.15% (e.g., Table 1).

Graphical representation of the analytical results

Because the starting materials for the synthetic samples are mixtures in the Fe-Ti-Cr-O system, the chemical compositions of the coexisting mineral phases are best represented in the Fe-Ti-Cr-O tetrahedron (Fig. 3). Two projections are used. Changes in the Fe:Ti:Cr ratios are revealed in a projection from the O apex onto the Fe-Ti-Cr triangle. Redox processes or changes in defect concentrations in spinel or ilmenite are best shown in a projection parallel to the $Fe_I^{2+}Ti_I^{4+}Cr_2^{3+}$ substitution lines onto the Fe-Ti-O triangle. The last projection scheme leads to a representation fully comparable to that used for Cr-free iron titanium oxides.

Note that in all diagrams the symbols represent the mean of 10–30 single analyses, and that their size corresponds to 2σ.

TABLE 2. Microprobe analyses of ulvöspinel from starting samples synthesized at 1300 °C under different f_{O_2} (means and standard deviations)

Sample	Ki-1/1	Ki-1/2	Ki-1/3	Ki-1/4	Ki-1/5
log f_{O_2}	−11.0	−10.0	−9.5	−9.0	−8.5
No. of analyses	$n = 13$	$n = 13$	$n = 14$	$n = 14$	$n = 11$
Ti (wt%)	20.29(8)	18.86(4)	18.10(5)	17.44(8)	15.93(6)
Cr	6.80(7)	7.59(10)	8.01(9)	8.23(9)	8.96(11)
Fe	43.42(22)	44.53(10)	44.86(13)	45.33(19)	46.17(15)
O	28.49(10)	28.28(7)	28.15(5)	28.07(10)	27.71(7)
Total	98.99(21)	99.26(17)	99.12(19)	99.07(19)	98.77(15)
Ti_{tot} (cat%)	31.81(16)	29.45(5)	28.30(8)	27.30(17)	24.98(11)
Cr	9.82(8)	10.93(14)	11.55(12)	11.86(12)	12.94(16)
Fe_{tot}	58.38(13)	59.62(11)	60.16(10)	60.85(14)	62.09(13)
OC (at%)	57.21(13)	56.93(8)	56.85(6)	56.81(12)	56.53(9)
FC (at%)	63.28(14)	65.09(4)	65.93(7)	66.78(14)	68.56(10)

Note: for explanations and abbreviations, see Table 1.

STARTING SAMPLES

The starting samples consist of polycrystalline, equigranular assemblages of ilmenite$_{ss}$ and ulvöspinel$_{ss}$ (Fig. 4). The size of the crystals is in the range 10–30 μm. In reflected light, spinel displays a uniform beige to light-gray color (depending on composition), whereas ilmenite is pleochroic from beige to light brown.

In each sample, both mineral phases have homogeneous compositions within the crystals and over the whole sample (cf. standard deviations in Tables 1 and 2 and the corresponding size of the symbols in Fig. 5). The compositions of coexisting ulvöspinel$_{ss}$ and ilmenite$_{ss}$ are clearly dependent on f_{O_2} (Fig. 5). With increasing f_{O_2}, from log $f_{O_2} = -11$ (i.e., 0.25 log unit below the iron + wüstite buffer; cf. O'Neill, 1988) to log $f_{O_2} = -8.5$ (0.65 log unit below the wüstite + magnetite buffer; cf. O'Neill, 1988), there is a clear increase in the FC ratio in both phases [Fig. 5a and 5b; FC = 100(Fe + ½Cr)/(Fe + Ti + Cr) in cation percent]. This reproduces the shift of the spinel-ilmenite tie lines toward the Fe side in the Cr-free system (see Fig. 2b), as shown by Webster and Bright (1961), Lindsley (1962, 1963), Grey et al. (1974), and Simons and Woermann (1978) at different temperatures and f_{O_2} ranges. This shift is correlated with decreasing Ti^{3+}- and increasing Fe^{3+}-contents in both phases, as shown by the ilmenite analyses (Table 1).

Moreover, the OC-ratio in coexisting ulvöspinel$_{ss}$ and ilmenite$_{ss}$ also depends on f_{O_2}, in contradiction with previous studies (e.g., Grey et al., 1974). The highest O values, i.e., the highest concentrations of cationic vacancies, are observed at the lowest f_{O_2} (Fig. 5a). In the case of

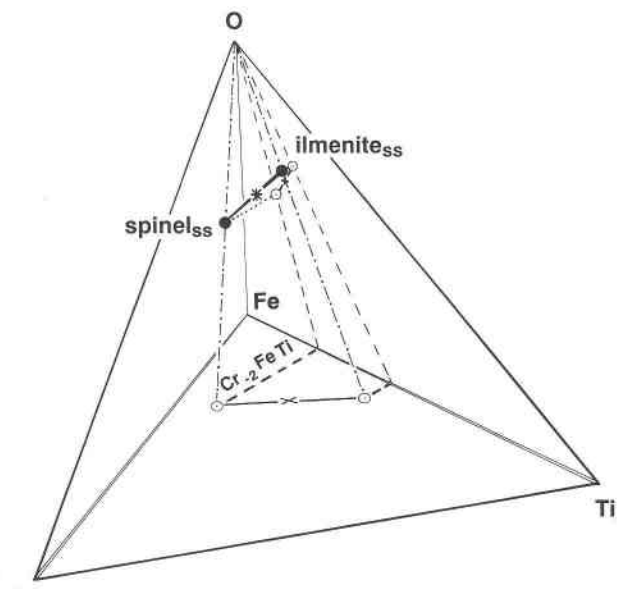

Fig. 3. Fe-Ti-Cr-O tetrahedron with locations of spinel$_{ss}$ and ilmenite$_{ss}$ (solid circles) and of their projections onto the Fe-Cr-Ti and the Fe-Ti-O planes (open circles). Note that in the latter case the projection is not from the Cr apex but, instead, performed parallel to the $Fe_1Ti_1Cr_{-2}$ exchange vector. The asterisk represents the bulk composition, the crosses its projections.

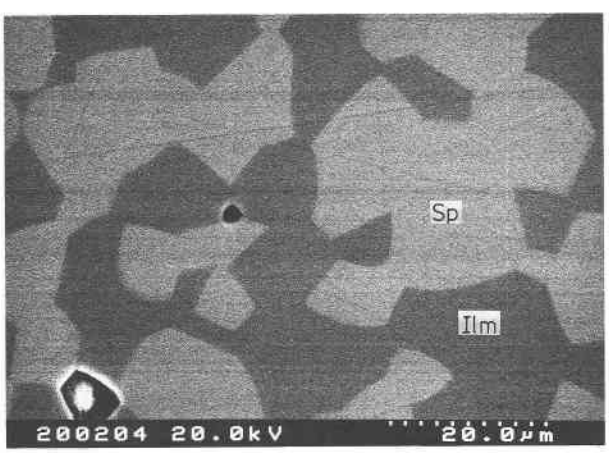

Fig. 4. Backscattered electron image of a starting sample (Ki-1/2, synthesized at 1300 °C, $f_{O_2} = 10^{-10}$; cf. Tables 1 and 2). Roughly equigranular crystals of ulvöspinel$_{ss}$ (light gray) and ilmenite$_{ss}$ (dark gray). The blackspots with white rims are pores. Images obtained with an S-4000 Hitachi field-emission scanning electron microscope, using an electron-gun accelerating voltage of 20 kV and a beam current in the range 0.03–0.09 nA (applies also to Figs. 6–8).

TABLE 3. Conditions and results of annealing experiments

Starting samples		Annealing				Textures in annealed samples				
							Ilm-exsol		Sp-exsol	
Expt.	log f_{O_2}	Expt.	T (°C)	t (d)	Assemblage	Type	Rims	Lam	Rims	Lam
Ki-1/1	−11.0	K 210v	1000	14	Sp + Ilm + (Fe°)	I	++	++	−	−
		K 211v	950	14	Sp + Ilm + (Fe°)	I	++	+++	−	−
		K 213v	850	90	Sp + Ilm + (Fe°)	I	++	+++	−	−
Ki-1/2	−10.0	K 6	1000	5	Sp + Ilm	II	++	+	−	−
		K 220v	1000	14	Sp + Ilm	II	+++	+	−	−
		K 221v	950	20	Sp + Ilm	II	+++	+	−	−
		K 223v	850	90	Sp + Ilm	II	+++	+	−	−
Ki-1/3	−9.5	K 241v	950	18	Sp + Ilm	II	+++	+	−	−
		K 242v	900	30	Sp + Ilm	II	+++	+	−	−
Ki-1/4	−9.0	K 9	1000	5	Sp + Ilm	II	+++	+	−	−
		K 232v	900	21	Sp + Ilm	II	+++	++	−	−
Ki-1/5	−8.5	K 40	1100	3	Sp + Ilm	III	++	+	−	−
		K 41	1000	5	Sp + Ilm	III	++	+	+	−
		K 251v	950	12	Sp + Ilm	III	+++	++	+	+
		K 253	850	20	Sp + Ilm	III	+	+++	+	+

Note: abbreviations: Ilm-exsol = exsolution of ilmenite within or around spinel crystals; Sp-exsol = exsolution of spinel within or around ilmenite crystals; Lam = lamellae; Ilm = ilmenite; Sp = spinel. Assemblage: phase in parentheses is present only in small amounts (<10 vol%). Textures: increasing abundance of rims or lamellae from "−" (absent) to "+++" (very abundant). Chemical changes during annealing: ΔCr(max) = maximal change in Cr-content measured (cation percent); ΔOC = OC (1300 °C) − OC (annealing); ΔFC = FC (1300 °C) − FC (annealing). The ΔOC and ΔFC are means (atom percent).

ilmenite$_{ss}$, the low OC ratio at $f_{O_2} = 10^{-8.5}$ might also result from a small concentration of interstitial cations.

ANNEALED SAMPLES

After annealing (at 700–1100 °C), the samples still consist of polycrystalline, roughly equigranular aggregates of spinel and ilmenite, with a grain size similar to that of the starting samples. In nearly all annealed samples, however, the spinel crystals display textures that are evocative of (and, as we will see, the result of) exsolution processes.

Chemical compositions of coexisting ulvöspinel$_{ss}$ and ilmenite$_{ss}$

The annealed samples display conspicuous differences in the chemical compositions of the coexisting ulvöspinel$_{ss}$ and ilmenite$_{ss}$ in comparison with the starting samples (Table 3). (1) The Cr contents are higher in spinel but lower in ilmenite (Table 3; e.g., Fig. 6c), which is related to the repartitioning of Cr through the strongly temperature-dependent exchange reaction $(FeCr_2O_4)_{Sp} + (FeTiO_3)_{Ilm} = (Fe_2TiO_4)_{Sp} + (Cr_2O_3)_{Ilm}$ (Knecht et al., 1977). In most annealed samples, the spinel crystals are zoned (Fig. 6c), i.e., the Cr-Fe-Ti exchange process did not reach equilibrium during the experiment. In contrast, the ilmenite crystals have generally homogeneous compositions within each crystal or lamella and over the whole annealed sample. This points to higher cation diffusion rates in ilmenite$_{ss}$ than in ulvöspinel$_{ss}$. (2) Both the FC and the OC ratios change in the spinel during annealing. In ilmenite, the changes are, in any case, smaller than in the spinel (Table 3). In contrast to the Cr contents, FC and OC ratios are, for both minerals, practically constant within each crystal and throughout the sample (Fig. 6b and 6c).

Correlation between exsolution textures and chemical composition of ulvöspinel$_{ss}$ and ilmenite$_{ss}$

As can be seen from Figure 6, the spinel/ilmenite modal ratio is not influenced by the Cr-Fe-Ti exchange but only by changes in the FC and OC ratios (ΔFC, ΔOC) in ulvöspinel$_{ss}$ and ilmenite$_{ss}$ (Fig. 6b and 6c). The ΔOC and ΔFC depend on the temperature and the duration of annealing and on the f_{O_2} during synthesis of the starting samples at 1300 °C. The last factor determines the type of exsolution, as described below. The exsolution types are numbered in order of increasing f_{O_2}.

Textures of type II. This textural type was observed in samples synthesized at f_{O_2} in the range 10^{-10}–10^{-9} (starting samples Ki-1/2, -1/3, -1/4; cf. Table 3). It is characterized by ilmenite rims around spinel crystals, often supplemented by single, relatively thick ilmenite lamellae, predominantly oriented in one set of {111} planes of the spinel (Fig. 6a).

Figure 6b and 6c show that, during annealing, spinel has not only gained Cr but has also increased its FC ratio and decreased its OC ratio (cf. also Table 3). The latter feature is best interpreted as a decrease in the concentration of cationic vacancies in spinel during annealing. In contrast, the ilmenite crystals and lamellae in the annealed samples have a lower Cr content but practically the same OC and FC ratios than the ilmenite of the corresponding starting sample.

In the Fe-Ti-O triangle, the spinel-ilmenite tie line for the annealed sample largely overlaps that of the starting sample (Fig. 6b). This means that the bulk composition, which is represented by the intersection of each tie line with the line of constant bulk FC ratio, has not changed during annealing, especially not in respect to its bulk OC ratio (Fig. 6b). This proves that annealing indeed took place under O_2-conserving conditions.

TABLE 3.—*Continued*

Chemical changes during annealing					
Δ Cr(max)		Δ FC		Δ OC	
Sp	Ilm	Sp	Ilm	Sp	Ilm
+3.87	−2.51	+2.36	+2.14	−0.76	−0.41
+7.71	−2.91	+2.97	+2.33	−0.85	−0.56
+9.62	−2.86	+2.90	+2.39	−0.63	−0.44
+3.46	−2.65	+0.88	+0.59	−0.12	+0.03
+4.23	−2.27	+2.56	+1.04	−0.78	−0.44
+4.06	−2.37	+2.41	+0.91	−0.58	−0.46
+2.98	−2.92	+1.73	+0.78		
+4.76	−2.65	+2.39	+0.34	−0.5	−0.01
+4.96	−2.71	+2.14	+0.31	−0.45	−0.01
+3.29	−2.63	+2.68	+0.25		
+2.21	−2.66	+1.53	−0.24		
+3.27	−2.24	+1.24	−0.44		
+4.06	−3.02	+1.78	−0.81		
+6.90	−3.01	+3.69	−0.60	−0.28	−0.21
+7.48	−2.78	+4.27	−0.07		

The modal proportions of spinel and ilmenite before and after annealing were estimated using the lever rule. For the example shown in Figure 6b, the molar proportions of ilmenite are 51% in the starting sample and 60% after annealing at 950 °C. Using, as a first approximation, the molar volumes of pure ilmenite (31.705 cm^3; Wechsler and Prewitt, 1984) and pure ulvöspinel (46.826 cm^3; Ishikawa et al., 1972), the modal proportion of ilmenite is 41 vol% in the starting sample but 50 vol% after annealing at 950 °C. These modal contents were checked by planimetry of BSE images from seven adjacent small surfaces (approximately 80 × 80 μm) in the respective samples, giving, in good agreement, 42 ± 4 and 51 ± 4 vol%.

Textures of type I. These textures appear only in the samples synthesized originally at the lowest f_{O_2} (10^{-11} at 1300 °C; starting sample Ki-1/1). They are characterized by small blebs of iron as well as abundant, trellis-like lamellae of ilmenite along several sets of {111} planes in the spinel crystals (Fig. 7a). The ilmenite rims around the spinel grains are irregular in thickness and resemble a pearl necklace. Lamellae and rims taken together represent a large amount of supplementary ilmenite that grew during annealing.

Indeed, increases in the FC ratio and decreases in the OC ratio during annealing affect not only the spinel but also the ilmenite (Table 3; Fig. 7b and 7c). For the example shown in Figure 7b this results in a change of the modal proportion for ilmenite from 29 vol% at 1300 °C to 43 vol% after annealing at 850 °C.

The appearance of iron after annealing is correlated with the shift of the three-phase-field spinel-ilmenite-iron toward Fe-richer compositions with decreasing temperature (see Fig. 2b and text). Because iron is present in the annealed sample, the bulk composition of the latter must lie within the spinel-ilmenite-iron triangle, and no oxidation should have occurred during annealing (Fig. 7b). On the basis of the phase relations alone, there could have been a slight reduction; but from an experimental point of view, it is difficult to imagine why any hypothetical reducing agent (traces of oil in the silica glass capsules?) would be active only in the samples synthesized under the lowest f_{O_2} and not in those of textural types II and III.

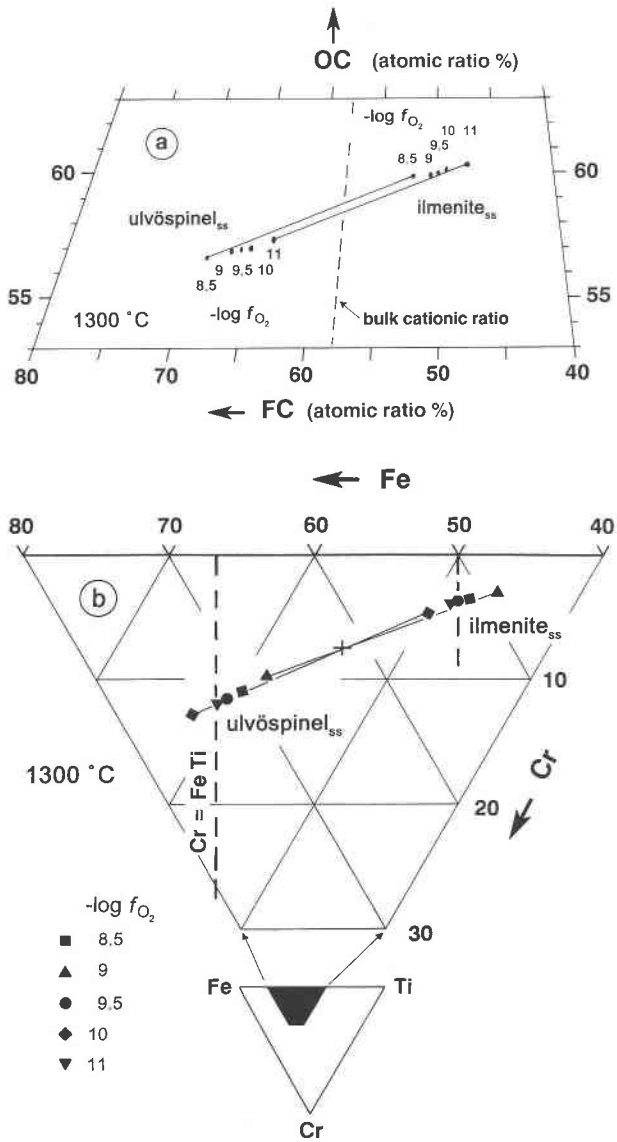

Fig. 5. Compositions of coexisting spinel and ilmenite (means, cf. Tables 1 and 2) in starting samples synthesized at 1300 °C and 1 atm under various oxygen fugacities. (**a**) Projection along the $Cr_{-2}Fe_1Ti_1$ substitution line onto the Fe-Ti-O plane (see Fig. 3). FC = 100(Fe +½Cr)/(Fe + Ti + Cr), OC = 100O/(O + Fe + Ti + Cr). Note that in the Cr-free system these FC and OC values are equivalent to those given in the caption of Fig. 1. The size of the symbols corresponds to 2σ. (**b**) Projection from the O apex onto the Fe-Ti-Cr plane. The size of the symbols corresponds approximately to 4σ.

Textures of type III. These textures were observed in the samples originally synthesized at the highest f_{O_2} ($10^{-8.5}$ at 1300 °C; starting sample Ki-1/5). The annealed samples present not only ilmenite rims and lamellae around

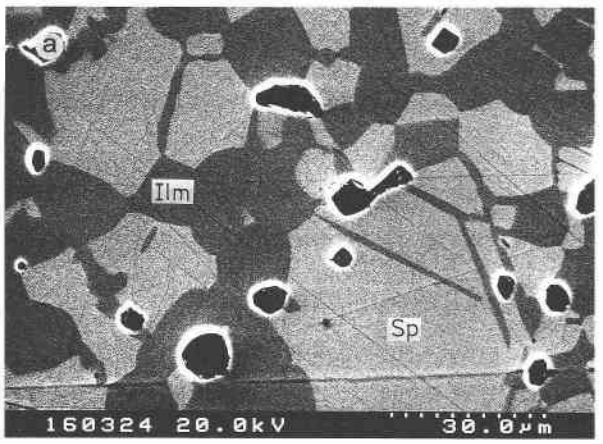

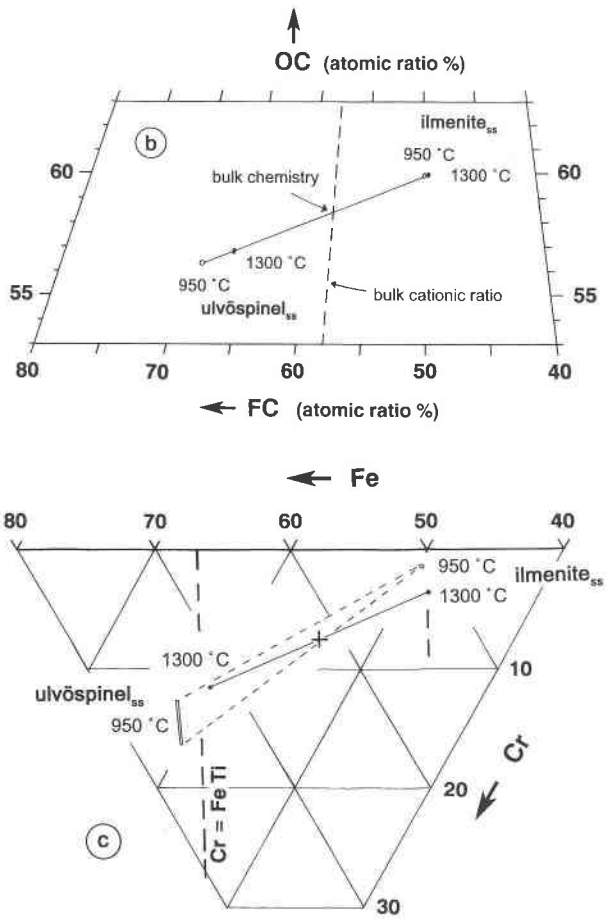

Fig. 6. Annealed sample K 241v (starting sample Ki-1/3, synthesized at 1300 °C, $f_{O_2} = 10^{-9.5}$; annealed at 950 °C for 18 d). (**a**) Backscattered electron image showing rims of ilmenite around spinel crystals and lamellae of ilmenite within a spinel crystal (textures of type II). (**b** and **c**) Chemical compositions of coexisting ulvöspinel$_{ss}$ and ilmenite$_{ss}$ in the annealed sample (open symbols) compared with those of the starting sample (dots). Same projections as in Fig. 5. Size of the symbols as in Fig. 5a.

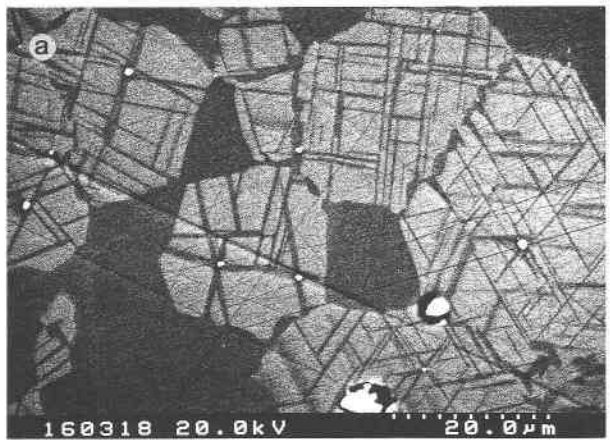

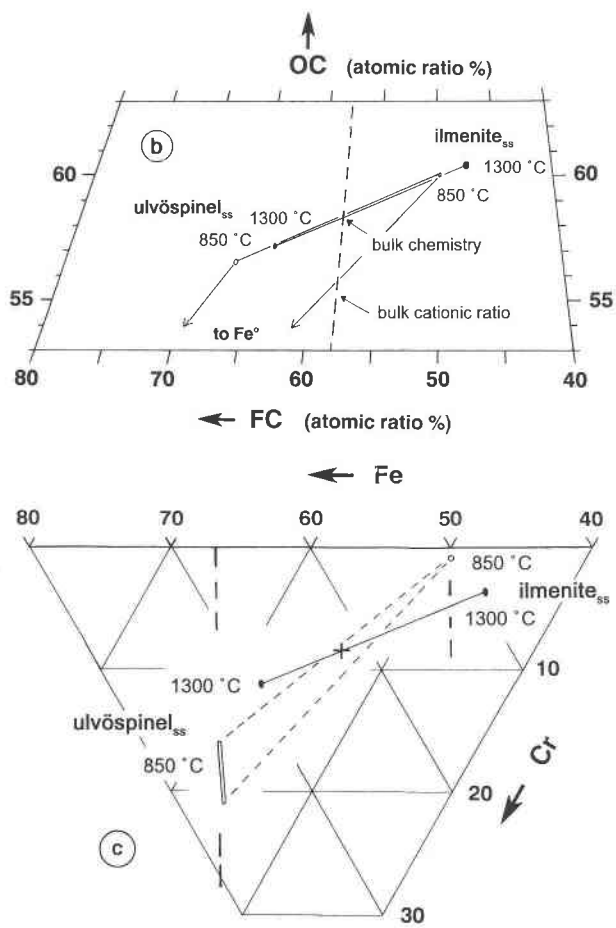

Fig. 7. Annealed sample K 213v (starting sample Ki-1/1, synthesized at 1300 °C, $f_{O_2} = 10^{-11}$; annealed at 850 °C for 90 d). (**a**) Backscattered electron image showing abundant ilmenite lamellae in all {111} planes of the spinel crystals (trellis-like) and discontinuous rims (resembling pearl necklace) of ilmenite between the spinel crystals. Note the small blebs of metallic iron (white). Representative example of textural type I. (**b** and **c**) Chemical compositions of coexisting ulvöspinel$_{ss}$ and ilmenite$_{ss}$ in the annealed sample (open symbols) compared with those in the starting sample (dots). Same projections as in Fig. 5.

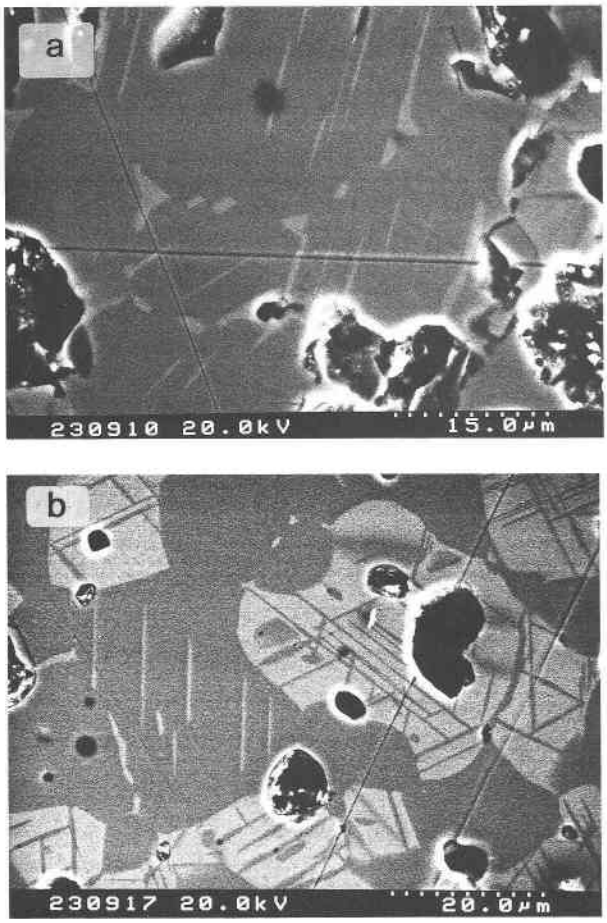

Fig. 8. Backscattered electron images showing representative exsolution textures of type III. The starting sample (Ki-1/5) was synthesized at 1300 °C, $f_{O_2} = 10^{-8.5}$. (**a**) Lamellae of spinel in the (0001) planes of ilmenite and discontinuous rims of spinel around the ilmenite crystals (sample K 250, annealed at 1000 °C for 32 h). Some lamellae merge in the discontinuous rims (e.g., upper right corner). (**b**) Abundant, trellis-like lamellae of ilmenite within spinel crystals and continuous rims of ilmenite between spinel crystals. In contrast, note the restricted amount of spinel lamellae in one set of planes within one ilmenite crystal and the small, discontinuous rims of spinel between some ilmenite crystals (sample K 253, annealed at 850 °C for 20 d).

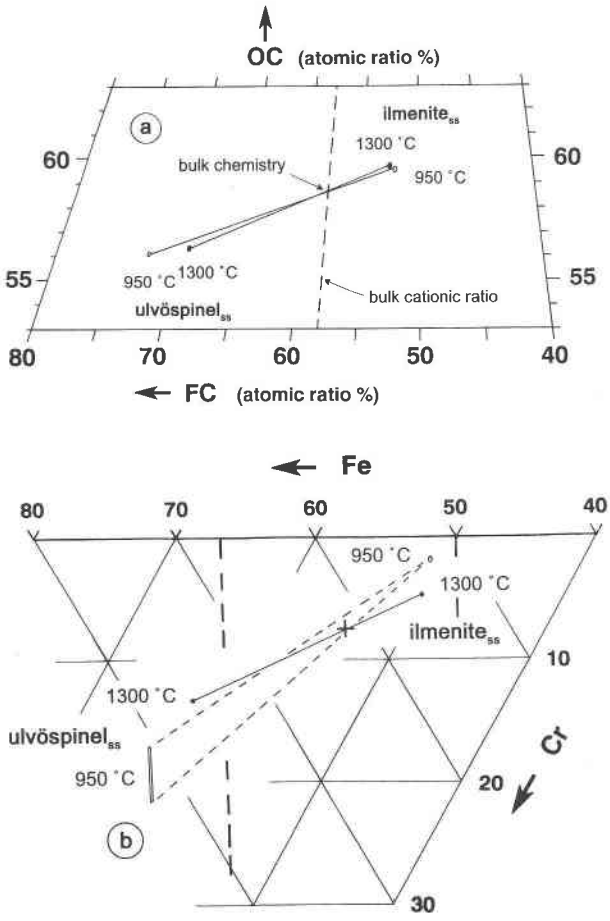

Fig. 9. (**a** and **b**) Chemical compositions of coexisting ulvöspinel$_{ss}$ and ilmenite$_{ss}$ in sample K 251v (open symbols; annealed at 950 °C for 12 d) compared with those of starting sample Ki-1/5 (dots). Same projections as in Fig. 5.

and within spinel crystals but also rims and lamellae of spinel around and along the (0001) planes of ilmenite crystals (Fig. 8a and 8b). The ilmenite lamellae are often of the trellis type, and the ilmenite rims are generally continuous and relatively broad (Fig. 8b). In contrast, the spinel rims are always discontinuous, forming small oval bodies (1–2 μm) dispersed along the grain boundaries and triangles at the triple-point junction (Fig. 8a and 8b). The spinel exsolution features are, however, less common than those of ilmenite and occur mainly in those parts of the samples with several adjacent ilmenite crystals. The amount of spinel exsolved from ilmenite is also smaller than the amount of ilmenite exsolved from spinel in the same sample.

The existence of spinel exsolution features matches mineral compositions. The ilmenite is characterized by lower FC ratios than those of the starting samples (Table 3; Fig. 9a and 9b). These lower ratios are compensated on a very local scale by the exsolution of small amounts of spinel (with much higher FC ratios). On the whole, however, the ilmenite/spinel modal ratio increases during annealing, as in all other samples. The compositional changes during annealing result in a clockwise rotation of the spinel-ilmenite tie line in the Fe-Ti-O diagram (Fig. 9a). Again, the crossing tie lines in the Fe-Ti-O triangle (Fig. 9a) indicate that the bulk chemistry did not change, i.e., that no redox process took place.

Vacancy relaxation as a mechanism for producing exsolution textures

The most important result of the microprobe analyses is that the exsolution features formed during annealing

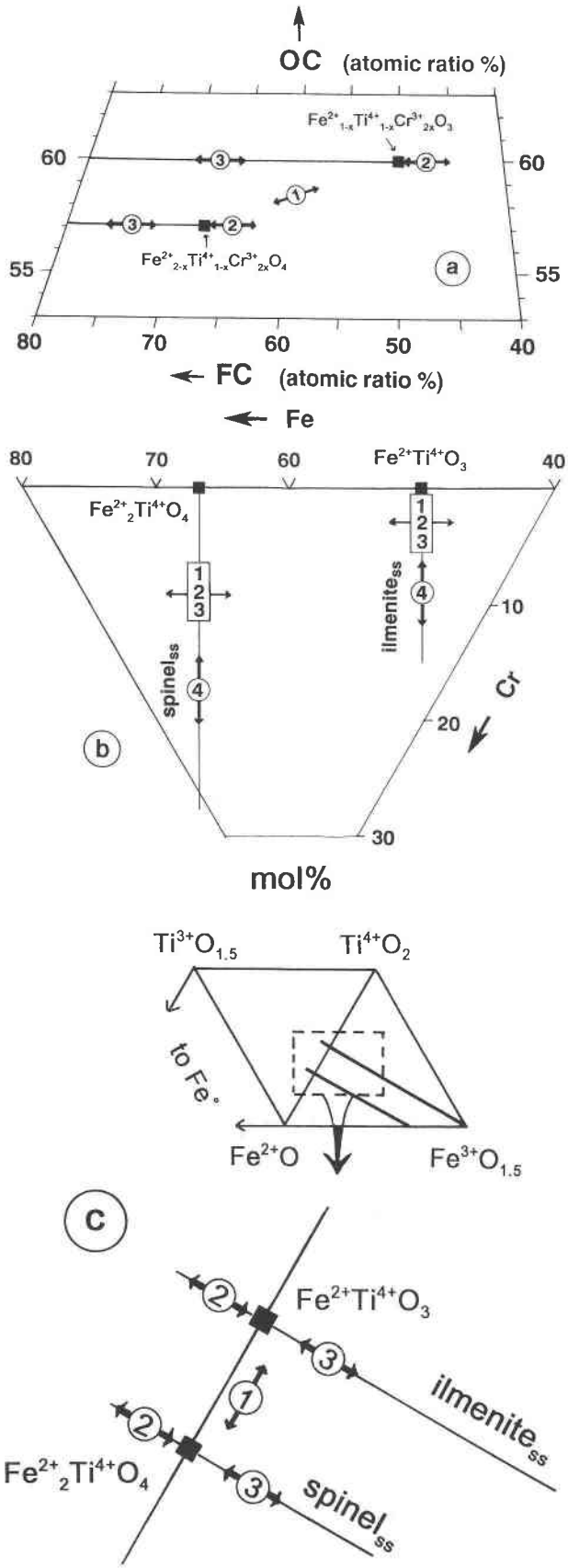

Fig. 10. Schematic representation of the effect of exchange reactions in spinel and ilmenite in the Fe-Ti-Cr-O system. The four exchanges are (1) $2Fe^{2+} = \square + Ti^{4+}$, (2) $Fe^{2+} + Ti^{4+} = 2Ti^{3+}$, (3) $Fe^{2+} + Ti^{4+} = 2Fe^{3+}$, (4) $Fe^{2+} + Ti^{4+} = 2Cr^{3+}$. (**a** and **b**) Same projections as in Fig. 5. (**c**) Double triangle FeO-TiO_2-$FeO_{0.5}$ and FeO-TiO_2-$TiO_{0.5}$, more commonly used in the petrological literature.

are not due to a redox process but are correlated with compositional changes in the coexisting ulvöspinel$_{ss}$ and ilmenite$_{ss}$, especially concerning their vacancy concentrations.

Substitution mechanisms in ulvöspinel and ilmenite solid solutions

In annealed samples exhibiting exsolution textures of both types I and II, the changes in the OC and FC ratios are such that the spinel-ilmenite tie line remains parallel to the tie lines at 1300 °C, i.e., to the $FeTiO_3$-Fe_2TiO_4 line. Therefore, the changes in the vacancy concentration in both phases must be controlled by the substitution $2Fe^{2+} = \square Ti^{4+}$ (Eq. 1) (see Fig. 10). Starting from the ulvöspinel and ilmenite end-members, this exchange leads to the defect end-members $Ti^{4+}_{2/3}\square_{1/3}O_4$ (defect spinel) and $Ti^{4+}_{1/3}\square_{0.5}O_3$ (defect ilmenite). Senderov et al. (1993) also reported that Exchange 1 "must be the only one effective for the formation of nonstoichiometric spinel on the FeO-TiO_2 join."

In the system Fe-Ti-Cr-O, three other substitutions can also occur:

$$Fe^{2+} + Ti^{4+} = 2Ti^{3+} \quad (2)$$

$$Fe^{2+} + Ti^{4+} = 2Fe^{3+} \quad (3)$$

$$Fe^{2+} + Ti^{4+} = 2Cr^{3+} \quad (4)$$

(see Fig. 10). During annealing, Exchange 4 is always operative between spinel and ilmenite (Knecht et al., 1977), but at least one of the other three exchange reactions also occurs: (a) In the case of textures of type II, only the spinel is affected by Exchange 1 during annealing. (b) In the more reduced assemblages ($f_{O_2} = 10^{-11}$ at 1300 °C), with textures of type I, both spinel and ilmenite experience a defect relaxation through Exchange 1 during annealing. Moreover, the Ti^{3+} content decreases in both phases through Exchange 2, which results in the appearance of iron by means of a sliding reaction. (c) Only in the more oxidized assemblages ($f_{O_2} = 10^{-8.5}$), with textures of type III, is Exchange 1 accompanied by Exchange 3. Spinel becomes enriched in Fe^{3+} (oxidized), whereas ilmenite loses Fe^{3+} (reduced). In the bulk there is no redox process but only a repartitioning of the Fe^{2+}, Ti^{4+}, and Fe^{3+} cations. Exchange 3 is operative only above a minimum f_{O_2}, which matches the observations of other authors (Lindsley, 1962, 1963; Spencer and Lindsley, 1981; Hammond et al., 1982).

Of course, many more substitution schemes could be written, e.g.,

$$3Fe^{2+} = \square + 2Cr^{3+} \quad (5)$$

$Ti^{3+} = Cr^{3+}$ . . . etc., but they all represent linear combinations of the four schemes discussed above. However, it must be stressed that these substitution schemes depict only overall chemical changes in the mineral phases without allocating the cations to any particular site in either the ilmenite or the spinel structure. From a crystal-chemical point of view, Exchange 5 is not necessarily equivalent to a combination of Exchanges 1 and 4 because they may involve different structural sites.

Estimates of vacancy concentrations in high-temperature (1300 °C) spinel and ilmenite

As discussed in the Analytical Methods section, direct calculations of the vacancy concentrations from the elemental concentrations are very sensitive to the accuracy of the latter. It is preferable to estimate the vacancy concentrations in the starting samples from changes in O content related to vacancy relaxation during annealing.

The following model reaction depicts a complete vacancy relaxation leading to a stoichiometric ulvöspinel: $Fe^{2+}_{2-2x}Ti^{4+}_{1+x}\square_xO_4 = 4xFe^{2+}Ti^{4+}O_3 + (1 - 3x)Fe^{2+}_2Ti^{4+}O_4$. The x value is related to the change in the OC ratio between defect and stoichiometric spinel by the equation $\Delta OC = 4/(7 - x) - 4/7$. In an analogous way, the formula of a defect ilmenite can be written as $Fe^{2+}_{1-2x}Ti^{4+}_{1+x}\square_xO_3$, and its vacancy concentration can be evaluated from $\Delta OC = 3/(5 - x) - 3/5$. All these equations are also valid for the solid solutions involved in the present study because Exchange 1 is the only one controlling the vacancy concentration in both ulvöspinel$_{ss}$ and ilmenite$_{ss}$.

Vacancy concentrations in the starting samples were calculated from all available ΔOC values (Table 4). The different results partly reflect incomplete vacancy relaxation because of slow reaction rates at relatively low annealing temperatures. But these results also confirm (Fig. 5a) that the vacancy concentrations are inversely correlated with the f_{O_2}, i.e., with the Fe-Ti ratios in coexisting ulvöspinel$_{ss}$ and ilmenite$_{ss}$ at 1300 °C. This is in accord with the results of Senderov et al. (1993) on a larger range of Fe/Ti values but contradicts Grey et al. (1974). It is also clear that the assumption of Aragon and McCallister (1982) of a stability field of zero width for the ulvöspinel end-member is no longer valid.

The vacancy ratios estimated here for Cr-bearing ilmenite and ulvöspinel$_{ss}$ are generally higher than those given in the literature for the Fe-Ti-O system (Table 5). Besides possible analytical discrepancies due to the different methods used, it is probable that the incorporation of Cr influences the vacancy concentration in ilmenite$_{ss}$ and ulvöspinel$_{ss}$. Previous analytical data (Knecht et al., 1977) show that the FC ratio decreases with increasing Cr content, especially in ilmenite but, to a smaller extent, also in spinel. This may be partly related to increasing Ti^{3+} contents but more probably to increasing vacancy contents according to Exchange 5, $3Fe^{2+} = \square + 2Cr^{3+}$. Al^{3+} seems to have a similar influence (Knecht, 1979). The incorporation of Zr^{4+} enhances the phase width of ilmenite but not that of ulvöspinel (Lattard, 1987), whereas Mg^{2+} reduces the phase widths of both minerals (Johnson et al., 1971; Knecht, 1979).

TABLE 4. Vacancy ratios in ulvöspinel$_{ss}$ and ilmenite$_{ss}$ from starting samples synthesized at 1300 °C, estimated from the ΔOC values in annealed samples

Annealing T (°C)	Vacancy ratios (at%)							
	Ki-1/1		Ki-1/2		Ki-1/3		Ki-1/5	
	Sp	Ilm	Sp	Ilm	Sp	Ilm	Sp	Ilm
1000	3.1	1.7	3.1	1.8				
950	3.4	2.3	2.3	1.9	2.0	0.0	1.1	0.9
900					1.8	0.0		
850	2.5	1.8						

PETROLOGICAL DISCUSSION

The experimental results presented above are especially relevant for highly reduced iron titanium oxide parageneses crystallized at high temperatures, i.e., in lunar rocks and some rare, iron-bearing terrestrial basalts (e.g., Pedersen, 1981). In such rocks, ilmenite lamellae within spinel and peripheral breakdown of ulvöspinel to iron + ilmenite (e.g., Medenbach and El Goresy, 1982) can be produced by exsolution processes, following the models of Ramdohr (1955) and Haselton and Nash (1975) (cf. Fig. 2a and 2b). It is, of course, possible that such textures result from reduction processes, as proposed by El Goresy et al. (1972) and Haggerty (1972, 1977) for lunar basalts, in accord with experimental studies in the Fe-Ti-O system (e.g., Taylor et al., 1972). These reduction models are, however, not very attractive because they rely on extraordinary reduction processes, including "solar wind containing H, N, C; late-stage outgassing of oxygen or sulfur from the lunar magma; a post-crystallization thermal event causing outgassing; or a reaction of oxides with iron carbonyls to produce metallic Fe^0 + CO" (quoted from Haselton and Nash, 1975; see citations in this article). Moreover, other features that were thought to reflect subsolidus reduction in lunar basalts may also be interpreted as caused by subsolidus reequilibration upon cooling. These include the decrease of the $TiO_2/(TiO_2 + Al_2O_3 + Cr_2O_3)$ ratio in spinel from core to rim (cf. El Goresy and Ramdohr, 1977) and the breakdown of ilmenite to rutile + iron (e.g., as described by El Goresy et al., 1972).

Because the vacancy concentration in iron titanium spinel apparently decreases with increasing f_{O_2}, i.e., increasing magnetite component (cf. Fig. 5a and also Senderov et al., 1993), vacancy relaxation is probably not responsible for the great majority of spinel + ilmenite microintergrowths in terrestrial igneous and metamorphic rocks. Also note that relatively low crystallization temperatures (T < 900 °C) further limit the original va-

TABLE 5. Cationic vacancies and interstitials in ulvöspinel$_{ss}$ and ilmenite$_{ss}$ as given in literature data

References	Phase (coex. with)	FT	$-\log f_{O_2}$	T (°C)	Fe^{2+}	Ti^{4+}	Ti^{3+}	Fe^{3+}	Σ cat	Vac	Vac(%)	Int	Int(%)
Shchepetkin et al. (1968)	Usp (Ilm-Fe°)			1000	1.95	1.03	—	—	2.98	0.02	0.7	—	—
	Ilm (Rut-Fe°)			1000	0.92	1.04	—	—	1.96	0.04	2		
Fetisov et al. (1969)	Ilm (Fpsb-Fe°)			1150	0.92	1.04	—	—	1.96	0.04	2	—	—
Grey et al. (1974)	Usp (Ilm-Fe°)		12.65	1200	1.95	1.02	—	—	2.97	0.03	1	—	—
	Ilm (Usp-Fe°)		12.65	1200	0.98	1.02	—	—	2.00	—	—	—	—
Simons and Woermann (1978)	Usp (Ilm-Fe°)	62.0	11.21	1300	1.897	1.034	0.024	—	2.955	0.045	1.5	—	—
		62.0	13.45	1130	1.929	1.024	—	0.015	2.968	0.032	1.1	—	—
		62.0	15.14	1000	1.892	0.994	—	0.080	2.966	0.034	1.1	—	—
	Ilm (Usp-Fe°)	62.0	11.21	1300	1.003	0.987	0.016	—	2.006	—	—	0.006	0.3
		62.0	13.45	1130	1.002	0.992	—	0.010	2.004	—	—	0.004	0.2
		62.0	15.14	1000	0.958	0.982	—	0.052	1.992	0.008	0.4	—	—
Senderov et al. (1993)	Usp (Fe°)	70.0	11.03	1300	1.932	0.933		0.135	3.000*	0.000*	0.0*	—	—
	Usp	70.0	10.06	1300	1.815	0.952	—	0.188	2.955	0.045	1.5	—	—
	Usp	70.0	9.04	1300	1.674	0.890	—	0.364	2.928	0.072	2.4	—	—
	Usp (Ilm)	66.7	9.07	1300	1.812	0.947	—	0.195	2.954	0.046	1.5	—	—
	Usp (Ilm)	66.7	9.49	1300	1.840	0.969	—	0.148	2.957	0.043	1.4	—	—
	Usp (Ilm)	66.7	10.00	1300	1.858	0.995	—	0.087	2.940	0.060	2.0	—	—
	Usp	66.7	11.17	1300	1.926	1.013	—	0.032	2.971	0.029	1.0	—	—
	Usp (Ilm)	60.0	11.00	1300	1.904	1.048	—	—	2.952	0.048	1.6	—	—

Note: abbreviations: FT = 100Fe/(Fe + Ti) (atom percent) of bulk composition; Σ cat = cation sum per formula unit; Vac = vacancies per formula unit; Vac(%) = vacancy ratio, i.e., 100Vac/(Vac + Σ cat); Int = interstitials per formula unit; Int(%) = 100Int/Σ cat. Structural formulae on the basis of four O atoms (ulvöspinel) or three O atoms (ilmenite).

* Reference sample, assumed by the authors to be stoichiometric, but probably slightly cation deficient because it does not coexist with wüstite.

cancy content. In most terrestrial rocks, spinel + ilmenite intergrowths are certainly best interpreted as the result of oxidation processes (Buddington and Lindsley, 1964; Haggerty, 1991a; Frost and Lindsley, 1991). The source for O_2 may, however, be reduction reactions in another subsystem of the rock (e.g., the fluid phase or silicates; cf. Frost, 1991), so that the whole process need not be related to O_2 input from an external source.

Considering the high temperatures and relatively low f_{O_2} prevailing in parts of the Earth's upper mantle, iron titanium oxides in this environment are also candidates for primary high-vacancy concentrations and subsequent exsolution, which could explain spinel lamellae in ilmenite observed in mantle xenoliths (e.g., Haggerty, 1991b). It is, however, unclear whether the high mantle pressures lower the vacancy contents (which could be expected) or have the opposite effect (as in the case of wüstite above ca. 100 kbar; cf. Liu, 1976; Shen et al., 1983). Any further speculation must await experimental work on iron titanium oxides at high to very high pressures.

ACKNOWLEDGMENTS

This study was initiated under the supervision of Eduard Woermann and supported at the Institut für Kristallographie at the RWTH (Technical University) in Aachen (Germany) by a grant from the Deutsche Forschungsgemeinschaft (Wo 81/22). The experiments were performed partly in Aachen and partly at the Mineralogisch-Petrographisches Institut at Kiel University. Technical help was provided in Aachen by Ute Zeininger. Microprobe work was performed in different institutions. Preliminary results were obtained at the Max-Planck-Institut in Heidelberg with the help of Herma Blank, Ahmed El Goresy, and Joachim Janicke and at the Ruhr-Universität Bochum with the help of W. Köhler-Schnettger. Microprobe work centered on the delicate oxygen determination was performed, with the help of Larryn Diamond, Anne Feenstra, and Ingo Sedler, at the Mineralogisch-Petrographisches Institut in Bern on a Cameca SX-50 microprobe financed by the Schweizerisches National Fonds (Credit 21-26579.89). The SEM images were obtained on an Hitachi S-4000 operated by U. Gernert at the "ZELMI" laboratory of the Technische Universität Berlin. Polished sections for microprobe and SEM work were prepared by Mr. Lemler (Heidelberg), A. Kessler, and M. Mieles (Bochum). This work profited from intensive discussions with E. Woermann during my time in Aachen. L. Diamond (Bern) and G. Franz (Berlin) provided very helpful comments. B.R. Frost (Laramie), S. Haggerty (Amherst), D.H. Lindsley (Stony Brook), and L.A. Taylor reviewed the final versions. The recommendations of B.R. Frost helped to condense drastically the paper and the comments of D.H. Lindsley to improve the presentation.

REFERENCES CITED

Andersen, D.J., and Lindsley, D.H. (1988) Internally consistent solution models for Fe-Mg-Mn-Ti oxides: Fe-Ti oxides. American Mineralogist, 73, 714–726.

Aragon, R., and McCallister, R.H. (1982) Phase and point defect equilibria in the titanomagnetite solid solution. Physics and Chemistry of Minerals, 8, 112–120.

Borowiec, K., and Rosenqvist, T. (1985) Phase relations and oxygen potentials in the Fe-Ti-Mg-O system. Scandinavian Journal of Metallurgy, 14, 33–43.

Buddington, A.F., and Lindsley, D.H. (1964) Iron-titanium oxide minerals and synthetic equivalents. Journal of Petrology, 5, 310–357.

Darken, L.S., and Gurry, R.W. (1945) The system iron-oxygen: I. The wüstite field and related equilibria. Journal of the American Chemical Society, 67, 1398–1412.

Deines, P., Nafziger, R.H., Ulmer, G.C., and Woermann, E. (1974) Temperature-oxygen fugacity tables for selected gas mixtures in the system C-H-O at one atmosphere total pressure. Bulletin of the Earth and Mineral Sciences Experiment Station, 88, 129 p.

Dieckmann, R. (1982) Defects and cation diffusion in magnetite (IV): Nonstoichiometry and point defect structure of magnetite ($Fe_{3-\delta}O_4$). Berichte der Bunsen Gesellschaft für physikalische Chemie, 86, 112–118.

El Goresy, A. (1976) Oxide minerals in lunar rocks. In Mineralogical Society of America Reviews in Mineralogy, 3, EG1–EG46.

El Goresy, A., and Ramdohr, P. (1977) Apollo 17 TiO_2-rich basalts: Reverse spinel zoning as evidence for subsolidus equilibration of the spinel-ilmenite assemblage. Proceedings of the Eighth Lunar Science Conference, Geochimica et Cosmochimica Acta, Supplement 8, 1611–1624.

El Goresy, A., Taylor, L.A., and Ramdohr, P. (1972) Fra Mauro crystalline rocks: Mineralogy, geochemistry and subsolidus reduction of the opaque minerals. Proceedings of the Third Lunar Science Conference, Geochimica et Cosmochimica Acta, Supplement 3, 333–349.

Ender, A. (1976) Stabilität der Pseudobrookitphase im System Fe-Ti-O im Gleichgewicht mit metallischem Eisen, 72 p. Studienarbeit thesis, RWTH Aachen, Germany.

Ender, A., Hofmann, R., Stapper, L., Dhupia, G., and Woermann, E. (1980) Die Stabilität von Pseudobrookitmischkristallen. Fortschritte der Mineralogie, 58, Beiheft 1, 26–27.

Fetisov, V.B., Leont'yev, L.I., Kudinov, B.Z., Men', A.N., and Chufarov, G.I. (1969) Thermodynamic analysis of the equilibrium during reduction of iron metatitanate with hydrogen. Russian Metallurgy, 5, 4–7.

Frondel, J.W. (1975) Lunar mineralogy, 323 p. Wiley, New York.

Frost, B.R. (1991) Introduction to oxygen fugacity and its petrologic importance. In Mineralogical Society of America Reviews in Mineralogy, 25, 1–9.

Frost, B.R., and Lindsley, D.H. (1991) Occurrence of iron-titanium oxides in igneous rocks. In Mineralogical Society of America Reviews in Mineralogy, 25, 433–468.

Ghiorso, M. (1990) Thermodynamic properties of hematite-ilmenite-geikielite solid solutions. Contributions to Mineralogy and Petrology, 104, 645–667.

Grey, I.E., and Merritt, R.R. (1981) Stability relations in the pseudobrookite solid solution $Fe_yTi_{3-y}O_5$. Journal of Solid State Chemistry, 37, 284–293.

Grey, I.E., Reid, A.F., and Jones, D.G. (1974) Reaction sequences in the reduction of ilmenite: 4. Interpretation in terms of the Fe-Ti-O and Fe-Mn-Ti-O phase diagrams. Transaction of the Institution of Mining and Metallurgy, 83C, 105–111.

Haggerty, S.E. (1972) Apollo 14: Subsolidus reduction and compositional variations of spinels. Proceedings of the Third Lunar Science Conference, Geochimica et Cosmochimica Acta, Supplement 3, 305–332.

——— (1977) Apollo 14: Oxide, metal, and olivine mineral chemistries in 14072, with a bearing on the temporal relationships of subsolidus reduction. Proceedings of the Eighth Lunar Science Conference, Geochimica et Cosmochimica Acta, Supplement 8, 1809–1829.

——— (1991a) Oxide textures: A mini-atlas. In Mineralogical Society of America Reviews in Mineralogy, 25, 129–219.

——— (1991b) Oxide mineralogy of the upper mantle. In Mineralogical Society of America Reviews in Mineralogy, 25, 355–416.

Hammond, P.L., Tompkins, L.A., Haggerty, S.E., Taylor, L.A., Spencer, J.J., and Lindsley, D.H. (1982) Revised data for coexisting magnetite and ilmenite near 1000 degrees C, NNO and FMQ buffers. Geological Society of America Abstracts with Programs, 14, 506.

Haselton, J.D., and Nash, W.P. (1975) A model for the evolution of opaques in mare lavas. Proceedings of the Sixth Lunar Science Conference, Geochimica et Cosmochimica Acta, Supplement 6, 747–755.

Ishikawa, Y., Sato, S., and Syono, Y. (1972) Neutron and magnetic studies of a single crystal of Fe_2TiO_4. Technical Report of the Institute for Solid State Physics, University of Tokyo.

Johnson, R.E., Woermann, E., and Muan, A. (1971) Equilibrium studies in the system MgO-"FeO"-TiO2. American Journal of Science, 271, 278–292.

Knecht, B. (1979) Phasengleichgewichte und Elementverteilungen zwischen Spinell und Ilmenit. Diplom thesis, Rheinisch-Westfälische Technische Universität, Aachen, Germany.

Knecht, B., Simons, B., Woermann, E., and El Goresy, A. (1977) Phase relations in the system Fe-Cr-Ti-O and their application in lunar thermometry. Proceedings of the Eighth Lunar Science Conference, Geochimica et Cosmochimica Acta, Supplement 8, 2125–2135.

Lattard, D. (1987) Subsolidus phase relations in the system Zr-Fe-Ti-O in equilibrium with metallic iron: Implications for lunar petrology. Contributions to Mineralogy and Petrology, 97, 264–278.

Lattard, D., and Woermann, E. (1987) Kinetics of sub-solidus re-equilibration between ilmenite and spinel in the system Fe-Ti-Cr-O, with relevance to lunar basalts. Terra Cognita, 7, 253.

Lindsley, D.H. (1962) Investigations in the system FeO-Fe_2O_3-TiO_2. Carnegie Institution of Washington Year Book, 61, 100–106.

——— (1963) Equilibrium relations of coexisting pairs of Fe-Ti oxides. Carnegie Institution of Washington Year Book, 62, 60–66.

——— (1991) Experimental studies of oxide minerals. In Mineralogical Society of America Reviews in Mineralogy, 25, 69–106.

Liu, L.-G. (1976) The high-pressure phases of $FeSiO_3$ with implications for Fe_2SiO_4 and FeO. Earth and Planetary Science Letters, 33, 101–106.

MacChesney, J.B., and Muan, A. (1961) Phase equilibria at liquidus temperatures in the system iron oxide-titanium oxide at low oxygen pressures. American Mineralogist, 46, 572–582.

Medenbach, O., and El Goresy, A. (1982) Ulvöspinel in native iron-bearing assemblages and the origin of these assemblages in basalts from Ovifak, Greenland, and Bühl, Federal Republic of Germany. Contributions to Mineralogy and Petrology, 80, 358–366.

Merritt, R.R., and Turnbull, A.G. (1974) A solid-state cell study of oxygen activities in the Fe-Ti-O system. Journal of Solid State Chemistry, 10, 252–259.

Nafziger, R.H., Ulmer, G.C., and Woermann, E. (1971) Gaseous buffering for the control of oxygen fugacity at one atmosphere. In G.C. Ulmer, Ed., Research techniques for high pressure and high temperature, p. 9–41. Springer, Berlin.

O'Neill, H.St.C. (1988) Systems Fe-O and Cu-O: Thermodynamic data for the equilibria Fe-"FeO," Fe-Fe_3O_4, "FeO"-Fe_3O_4, Fe_3O_4-Fe_2O_3, Cu-Cu_2O, and Cu_2O-CuO from emf measurements. American Mineralogist, 73, 470–486.

Pedersen, A.K. (1981) Armalcolite-bearing Fe-Ti oxide assemblages in graphite-equilibrated salic volcanic rocks with native iron from Disko, Central West Greenland. Contributions to Mineralogy and Petrology, 77, 307–324.

Pouchou, J.L., and Pichoir, F. (1984) Un nouveau modèle de calcul pour la microanalyse quantitative par spectrométrie de rayons X. La Recherche Aérospatiale, 3, 167–192.

Ramdohr, P. (1955) Die Erzmineralien und ihre Verwachsungen, 875 p. Akademie Verlag, Berlin.

Senderov, E., Dogan, A.U., and Navrotsky, A. (1993) Nonstoichiometry of magnetite-ulvöspinel solid solutions quenched from 1300 °C. American Mineralogist, 78, 565–573.

Shchepetkin, A.A., Antonov, V.K., Dvinin, V.T., and Chufarov, G.I. (1968) Crystal chemical changes in the dissociation of iron titanate Fe_2TiO_4 under equilibrium conditions. Russian Journal of Inorganic Chemistry, 13, 1633–1634.

Shen, P., Bassett, W.A., and Liu, L.-G. (1983) Experimental determination of the effects of pressure and temperature on the stoichiometry and phase relations of wüstite. Geochimica et Cosmochimica Acta, 47, 773–778.

Simons, B., and Woermann, E. (1978) Iron titanium oxides in equilibrium with metallic iron. Contributions to Mineralogy and Petrology, 66, 81–89.

Spencer, K.J., and Lindsley, D.H. (1981) A solution model for coexisting iron-titanium oxides. American Mineralogist, 66, 1189–1201.

Taylor, L.A., Williams, R.J., and McCallister, R.H. (1972) Stability relations of ilmenite and ulvöspinel in the Fe-Ti-O system and application of these data to lunar mineral assemblages. Earth and Planetary Science Letters, 16, 282–288.

Taylor, R.W. (1964) Phase equilibria in the system FeO-Fe_2O_3-TiO_2 at 1300 °C. American Mineralogist, 49, 1016–1030.

Webster, A.H., and Bright, N.F.H. (1961) The system iron-titanium-oxygen at 1200 °C and oxygen partial pressures between 1 atm. and 2×10^{-14} atm. Journal of the American Ceramic Society, 44, 110–116.

Wechsler, B.A., and Prewitt, C.T. (1984) Crystal structure of ilmenite ($FeTiO_3$) at high temperature and at high pressure. American Mineralogist, 69, 176–185.

Manuscript received August 12, 1994
Manuscript accepted May 24, 1995